AGU PUBLICATIONS

JGR

Journal of Geophysical Research: Oceans

RESEARCH ARTICLE

10.1002/2017JC013655

Key Points:
- Accounting for ENSO and PDO variability does not affect the type of noise model that best describes the sea-level trend residual
- Standard errors may be under (or over) estimated by assuming an AR(1) noise model when compared to a more realistic noise model
- The observed trend in the satellite altimetry era emerges from the intrinsic noise for some key locations in the Indian and Pacific Oceans

Supporting Information:
- Supporting Information S1
- Table S3
- Data Set S1

Correspondence to:
S. Royston,
sam.royston@utas.edu.au

Citation:
Royston, S., Watson, C. S., Legrésy, B., King, M. A., Church, J. A., & Bos, M. S. (2018). Sea-level trend uncertainty with Pacific climatic variability and temporally-correlated noise. *Journal of Geophysical Research: Oceans*, *123*, 1978–1993. https://doi.org/10.1002/2017JC013655

Received 23 NOV 2017
Accepted 20 FEB 2018
Published online 13 MAR 2018

Sea-Level Trend Uncertainty With Pacific Climatic Variability and Temporally-Correlated Noise

Sam Royston[1], Christopher S. Watson[1], Benoît Legrésy[2,3], Matt A. King[1], John A. Church[4], and Machiel S. Bos[5]

[1]Discipline of Geography and Spatial Sciences, University of Tasmania, Hobart, TAS, Australia, [2]CSIRO Oceans and Atmosphere, Hobart, TAS, Australia, [3]Antarctic Climate and Ecosystems Cooperative Research Centre, Hobart, TAS, Australia, [4]Climate Change Research Centre, University of New South Wales, Sydney, NSW, Australia, [5]Space and Earth Geodetic Analysis Lab, University of Beira Interior, Covilhã, Portugal

Abstract Recent studies have identified climatic drivers of the east-west see-saw of Pacific Ocean satellite altimetry era sea level trends and a number of sea-level trend and acceleration assessments attempt to account for this. We investigate the effect of Pacific climate variability, together with temporally-correlated noise, on linear trend error estimates and determine new time-of-emergence (ToE) estimates across the Indian and Pacific Oceans. Sea-level trend studies often advocate the use of auto-regressive (AR) noise models to adequately assess formal uncertainties, yet sea level often exhibits colored but non-AR(1) noise. Standard error estimates are over- or under-estimated by an AR(1) model for much of the Indo-Pacific sea level. Allowing for PDO and ENSO variability in the trend estimate only reduces standard errors across the tropics and we find noise characteristics are largely unaffected. Of importance for trend and acceleration detection studies, formal error estimates remain on average up to 1.6 times those from an AR(1) model for long-duration tide gauge data. There is an even chance that the observed trend from the satellite altimetry era exceeds the noise in patches of the tropical Pacific and Indian Oceans and the south-west and north-east Pacific gyres. By including climate indices in the trend analysis, the time it takes for the observed linear sea-level trend to emerge from the noise reduces by up to 2 decades.

Plain Language Summary We have made improved estimates of the time it takes for a trend signal to emerge from the inherent noise in sea level time series, in the Indian and Pacific Oceans. Sea level has been measured by satellites for over 20 years. There are apparent trends where sea level appears to be rising more in the west and central Pacific Ocean and rising less quickly along the US coast in this period, but these differences are due to long-period climate variability. Additionally, sea-level time series show strong temporal-correlation, meaning each value is affected by previous values in time. We combine this knowledge to make improved estimates of the trend and residual noise in the sea-level time series and discuss the time it takes for the observed trend to emerge from the inherent noise. Including climate variability in the assessment can reduce this time-of-emergence by up to 2 decades. There is an even chance that the observed trend from the satellite altimetry era (1993-2015) exceeds the noise in patches of the tropical Pacific and Indian Oceans and the south-west and north-east Pacific gyres.

1. Introduction

A key issue when deriving robust local sea-level trends is the presence of interannual and decadal period signals which mask the true long-term trend, particularly in relatively short instrumental records. This phenomenon is well evidenced by the apparent east-west see-saw of sea-level linear trends across the Pacific derived from satellite altimetry observations. This pattern in the sea-level trends from two decades of satellite observations can be largely explained by interannual and decadal basin-scale variability forced by internal climatic variability (Zhang & Church, 2012, hereinafter ZC12). Attempts have been made to account for, or remove, intrinsic climatic variability in the Pacific Ocean and elsewhere in studies involving linear trend estimation and detection of acceleration (Calafat & Chambers, 2013; Haigh et al., 2014; Hamlington et al., 2012); in mean sea-

level reconstructions (Hamlington et al., 2011); and, in attempts to separate natural and anthropogenic signals (Calafat & Chambers, 2013; Dangendorf et al., 2015; Hamlington et al., 2014; Meyssignac et al., 2012).

In the vast majority of these types of sea-level studies, uncertainty estimation involves the assumption that the residual exhibits either white noise (with an adjustment for the effective degrees of freedom in the presence of temporally-correlated noise) or order 1 auto-regressive noise, AR(1). However, sea-level time series exhibit temporal correlation with long-term memory (Dangendorf et al., 2014). When considering periods from wind wave (∼5 s) to geological (millenial), sea-level time series exhibit a power-law relationship with spectral index around −2 (Harrison, 2002), although a Monte Carlo test by Bos et al. (2014) demonstrated that for most sea-level time series a nonrandom-walk stochastic model is correct. Hughes and Williams (2010) consider the trend in global satellite altimetry sea-level measurements at periods of 2–24 weeks, finding an order 5 auto-regressive, AR(5), model is required to characterize the residual noise when fitting a linear trend for the majority (88%) of gridded sea-level anomalies. However, for long-duration tide gauge time series and global mean sea-level observations and reconstructions, a variety of different noise models have been found to best fit the residual (Bos et al., 2014; Burgette et al., 2013), all exhibiting temporal correlation.

Auto-correlation can significantly increase formal trend uncertainty estimates, affecting confidence in conclusions relating to the detection of sea-level acceleration and the anthropogenic signal. Here we examine the stochastic nature of the noise from linear trend estimation of sea-level from tide gauge and satellite altimetry data, over three different durations from 105 to 22.7 years, including key Pacific climate variates in the trend estimation and discuss formal trend error estimates. We demonstrate the effect of Pacific Decadal Oscillation (PDO) and El Niño South Oscillation (ENSO) variability and stochastic noise on the time of emergence (ToE) of a linear trend in sea level; the length of data required for a given trend to emerge from the intrinsic noise of the system. The implications for trend detection from satellite altimetry and long period tide gauge data are subsequently discussed.

2. Data

2.1. Altimeter Data

Along-track Level 3 altimeter data were used. The Level 3 DUACS altimeter data were procured from AVISO, which is now continued by CMEMS (Mertz et al., 2017). The unfiltered version of the Level 3 reprocessed data were stacked for every track segment over all available Topex/Poseidon, Jason-1 and OSTM/Jason-2 cycles. We only used data from the reference mission on the reference track which gives continuity and regularity in the downstream computations. The DUACS processing use all standard geophysical product corrections. Sea level anomalies were aligned and averaged along-track at 6 km equal spacing commencing at the equatorial crossing and following the nominal ground track. Here we focus on sea level time series across the Indian and Pacific Oceans. The time series covers the period 1 January 1993 to 10 September 2015 at the nominal 9.9156 day repeat pass interval. For computational efficiency we downsample to every 5 samples along-track, giving a nominal along-track spatial resolution of ∼30 km. The duration of satellite observations now available (22.7 years of data in this study) may approach an adequate length to confidently detect a linear trend of 2 mm a^{-1} across most ocean basins except the most energetic regions (Figure 3 of Jordá, 2014). Our focus here is to investigate the effect of climatic and intrinsic variability on this detection time.

The mean of the time series for each calendar month is also calculated for each along-track satellite altimetry time series. We only present results from sea-level time series with more than 67% completeness over the epochs studied.

2.2. Tide Gauge Data

Tide gauge records from the Indian and Pacific Oceans of monthly-mean sea-level from the Permanent Service for Mean Sea Level (PSMSL; Holgate et al., 2013; PSMSL, 2017) are truncated to the period January 1993 to September 2015 coincident with the altimetry data. Additionally, we investigate two longer epochs of monthly mean tide gauge time series, one epoch starting arbitrarily in 1960 and ending in 2015, and the longest epoch starting arbitrarily in 1900 and ending in 2005 due to the limited length of the extended multivariate ENSO time series, described below.

We have filled gaps up to 2 months in the tide gauge time series by a spline regression and reject tide gauge records where the time series has low correlation (<0.8) with all neighbouring tide gauge time series

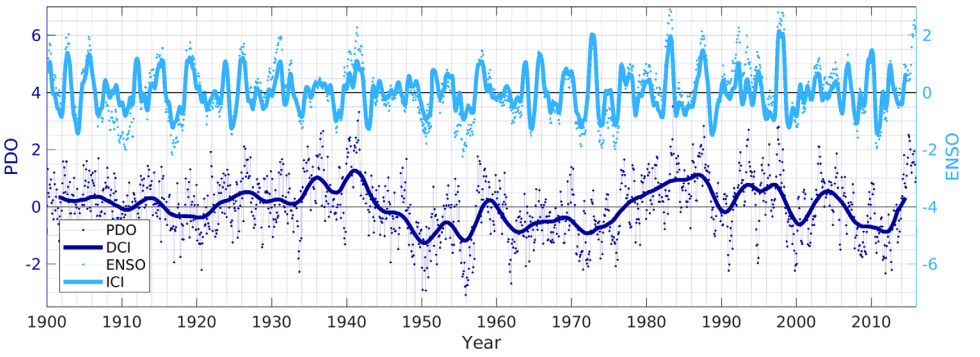

Figure 1. Time series of the Pacific Decadal Oscillation (PDO, monthly), multivariate El Niño Southern Oscillation (ENSO, bimonthly), filtered Decadal Climate Index (DCI) and Interannual Climate Index (ICI) used in this study.

(within a 2° box). All sites that are flagged by PSMSL are removed. Further manual amendments have been made to long duration tide gauge sites, as described in supporting information Table S1.

This data manipulation and completeness criteria reduces the tide gauge data set in the Indo-Pacific region to 22, 176 and 321 monthly time series for the epochs 1900–2005, 1960–2015 and 1993–2015 respectively and the satellite altimetry data to 55,776 time series.

2.3. Climate Data

Two major modes of Pacific climate variability, identified by ZC12 to account for much of the sea-level pattern across the Pacific, are used in this study. The Pacific Decadal Oscillation index (Mantua, 2016; Zhang et al., 1997) and the multi-variate and extended multi-variate ENSO indices (NOAA ESRL, 2016a, 2016b; Wolter & Timlin, 1993, 2011) have been filtered to isolate the spectral frequencies of an Interannual Climate Index (ICI) from those of a Decadal Climate Index (DCI). These indices have been interpolated to the monthly and 9.9 day repeat frequency of the sea-level data. Figure 1 presents the PDO and ENSO time series and the filtered DCI and ICI used in this study. It is noted that due to the filtering applied to these indices, the large El Niño event that peaked in the later months of 2015 is not included in this analysis.

3. Method

3.1. Regression

We analyze each sea-level time series (monthly tide gauge and monthly and 9.9 day repeat satellite altimetry) multiple times considering the effects of regressing against the DCI and ICI climate indices and various noise models. Total sea-level time series are decomposed by maximum likelihood estimation (MLE) regression into component terms:

$$\mathrm{SL}_i = \alpha_0 + \alpha_1 t + \alpha_2 \cos(2\pi t + \phi_a) + \alpha_3 \cos(4\pi t + \phi_{sa}) + \epsilon \quad (1)$$

where α_0 is a bias or offset term, α_1 is the linear trend in time, $\alpha_2, \alpha_3, \phi_a, \phi_{sa}$ are the amplitude and phase of the annual and semi-annual periodic signals respectively and ϵ is the residual noise. Hereafter, equation (1) is referred to as 'standard regression'.

The influence of Pacific climatic variability on the interannual to decadal scale is investigated using the approach of ZC12, where a multivariate regression including the DCI and ICI climate indices as variates is applied to each time series. The independence of the DCI and ICI time series is ensured by filtering (here the only difference to ZC12 is the application of a Butterworth filter to the PDO time series rather than a running mean, to better separate low and high frequencies):

$$\mathrm{SL}_i = \alpha_0 + \alpha_1 t + \alpha_2 \cos(2\pi t + \phi_a) + \alpha_3 \cos(4\pi t + \phi_{sa}) + \alpha_4 \mathrm{DCI} + \alpha_5 \mathrm{ICI} + \epsilon \quad (2)$$

Parameters in equations (1) and (2) are estimated using Hector, a freely available and fast MLE software (Bos et al., 2013). The capabilities of the software were extended for this study to allow multivariate analysis including climate indices. The design matrix was augmented with two columns that were filled with the DCI

and ICI values for the same epochs as the observations. The rest of the least-squares and MLE process remained the same.

We repeated the regression with five different stochastic noise model types: white noise and four different colored plus white noise models. In the spectral frequency domain, power-law noise is proportional to frequency to the exponent κ, $P(f)=P_0(f/f_0)^{\kappa}$ where P_0 and f_0 are constants. The value of κ is mostly smaller than zero which implies high power at low frequencies and low power at high frequencies. The auto-regressive (AR) noise model describes stochastic processes where the noise is determined by the immediate previous noise value(s) plus a white noise value. On a log-log power spectral density, AR(1) noise follows a linear trajectory with $\kappa=-2$ at high frequencies, flattening to a constant power at lower frequencies. The auto-regressive fractionally-integrated moving-average (ARFIMA) model additionally allows for integration of and moving average in the noise, which can model nonstationarity. The inclusion of the fractional integration means that the slope in the power spectral domain can take any value, whilst the auto-regressive part dictates there remains a change of slope at some crossover frequency. A generalized form of auto-regressive and integrated noise model was proposed by Langbein (2004) and is referred to as the generalized Gauss Markov (GGM) noise model. This generalized stochastic model has two parameters that fit the auto-regressive order and power-law exponent. On a log-log power spectral density plot, the GGM model has a linear slope which flattens to a constant power at low and very high frequencies. In this study we use the colored noise models AR(1) plus white; ARFIMA $(1, d, 0)$ plus white; GGM plus white; and, power-law plus white. Here d is proportional to the spectral index by $\kappa=-2d$. The MLE fits parameters to each of these models, with the approach described fully in Bos et al. (2013) and Bos and Fernandes (2016).

The appropriateness of a given stochastic noise model is assessed through the Akaike Information Criteria (AIC; Akaike, 1973) and Bayesian Information Criteria (BIC; Schwarz, 1978). For each time series each noise model is scored by the lowest values of the AIC and BIC and the score is scaled by the range of AIC or BIC values for each regression. This scaling takes into account slight (<2), moderate (2–6) and strong (>6) differences between the BIC values for each noise model. The most appropriate noise model is then determined as that with the lowest mean score of both the AIC and BIC. For most time series, the most appropriate model is judged the same by both the AIC and BIC.

For computational efficiency many sea-level trend studies have used a simplified least squares approach to determine sea-level trend estimates and the uncertainty of that linear trend estimate. In this approach, the effect of auto-correlation in the residuals on the trend error estimate is accounted for, by reducing the number of degrees of freedom in the standard error calculation (because the n observations are not independent in time; Emery & Thomson, 2001; von Storch & Zwiers, 1999). Whereas the MLE trend error estimate is derived explicitly from the observation covariance matrix and varies with the parameterization of each noise model (Bos et al., 2008).

3.2. Time of Emergence

We also consider the time of emergence (ToE), here taken to mean the duration of record needed for a given trend to exceed a surrogate stochastic noise time series based on our optimal noise model for each time series. Particularly with the growing focus on predicting local to regional sea-level change for adaptation and mitigation purposes, ToE is an important metric to diagnose when a signal emerges from the noise of the system. In this case, we assume the linear trend is the signal of interest (which may be of long-period natural or anthropogenic origin) and remove the variability from PDO and ENSO by multivariate linear regression. We subsequently identify when the observed trend signal exceeds the remaining noise in the system at each time series location.

We determine when a trend signal emerges from the noise following a similar approach to that used in studies to detect anthropogenic signals in global climate models (GCM) sea-level projections (e.g., Lyu et al., 2014). For each location, and for fixed noise model parameters derived by MLE regression with and without climate indices, we calculate 1,000 surrogate stochastic noise time series of 100 year length using Hector. The noise is simulated by the convolution of an impulse response with white noise, using FFT, which implicitly assumes the noise is zero before the first observation. Therefore for the power-law noise model, the surrogates include a spin-up of 1,000 time steps to allow the appropriate growth of representative low frequency noise. Note that for GCM projections, the ToE method usually compares a multi-model ensemble mean with the ensemble spread of 'natural' model runs. Here we determine the time taken for a trend to

exceed each surrogate noise time series. The time taken for a given target trend, of 0.5 to 10 mm a^{-1} to exceed each surrogate noise time series give a distribution of the ToE for each target trend, at each location (refer to supporting information Figures S1 and S2). For the satellite altimetry era, here covering 22.7 years, we apply a spline interpolation on the probability distribution of ToE for a given location and noise model to determine what magnitude of trend exceeds the noise, and compare against the observed trend from the satellite altimetry era. This is because we want to capture the influence of the colored nature of the noise, where the noise signal may grow in time. As a result, the method applied here gives longer ToE than applying a signal to noise ratio where the noise threshold is two standard deviations.

It is noted that, due to the larger variability in observations compared with GCM and noting that the along-track satellite altimetry data here are not spatially smoothed, the ToE derived here are expected to be longer than those determined from previous studies of observations and GCM.

An alternative approach is commonly used in observed sea-level rise detection and attribution studies (e.g., Haigh et al., 2014; Jordá, 2014; Richter & Marzeion, 2014), where the apparent trend is calculated for each surrogate noise time series for different sizes of sliding window, giving an apparent ToE for a given magnitude of trend. However, applying this approach to determine the trend by MLE with the most appropriate noise model for each time series is too computationally expensive when applied to the large number of sea-level time series investigated here.

From the ToE distributions, the detectable trend for a given duration of record is calculated by spline interpolation on the implied confidence intervals of the 50th, 75th and 95th percentile of the distribution.

This approach identifies the time at which an observed signal becomes detectable beyond the known explainable variables and residual noise.

4. Results and Discussion

4.1. Noise in Regression When Including Climate Variability

Varying the duration of data coverage and sample frequency of the sea-level time series affects the spectral shape of the residual noise. Linear regression on shorter time series are prone to overestimating the linear trend, by assigning variance due to long-period oscillations (long relative to the sample data length) to the trend rather than the noise term. For observations that include long period variability, it is therefore expected that the noise spectra from longer duration samples should exhibit higher power at the lowest frequency than a shorter sample of the same data. If the longer period oscillations in sea level are dominated by PDO and ENSO climate variability, it would be expected that including these variates in a linear regression would reduce the power in the noise at the longest period for all sample lengths, changing the shape of the spectra.

Figure 2 presents the proportion of each data set best described by each noise model (values are provided in supporting information Table S2) and Figure 3 presents these proportions binned by latitude bands for the satellite altimetry data and coincident epoch of tide gauge data. The duration and sampling frequency of the sea-level time series has a significant effect on the most appropriate noise model, determined through the mean AIC/BIC score.

For the longest duration tide gauge time series from the epoch 1900–2005, every site exhibits colored noise and for 77% (63%) of sites the noise is best described by a non-AR(1) model, when including (excluding) climate indices in the regression.

For the 55 year duration tide gauge time series from the epoch 1960–2015, every site exhibits colored noise but the proportion of sites best described by AR(1) noise is greater than the longest duration data. For 33% (48%) of sites, the noise is best described by a non-AR(1) model, when including (excluding) climate indices in the regression.

For both the tide gauge data and the monthly satellite altimetry data over the 1993–2015 epoch, the majority of the time series display white or AR(1) noise (71–87% of time series are best described by white or AR(1) noise with the range depending on the sea-level observation method and the inclusion or not of climate indices in the regression). However, the noise in the satellite altimetry data at its original 9.9156 day

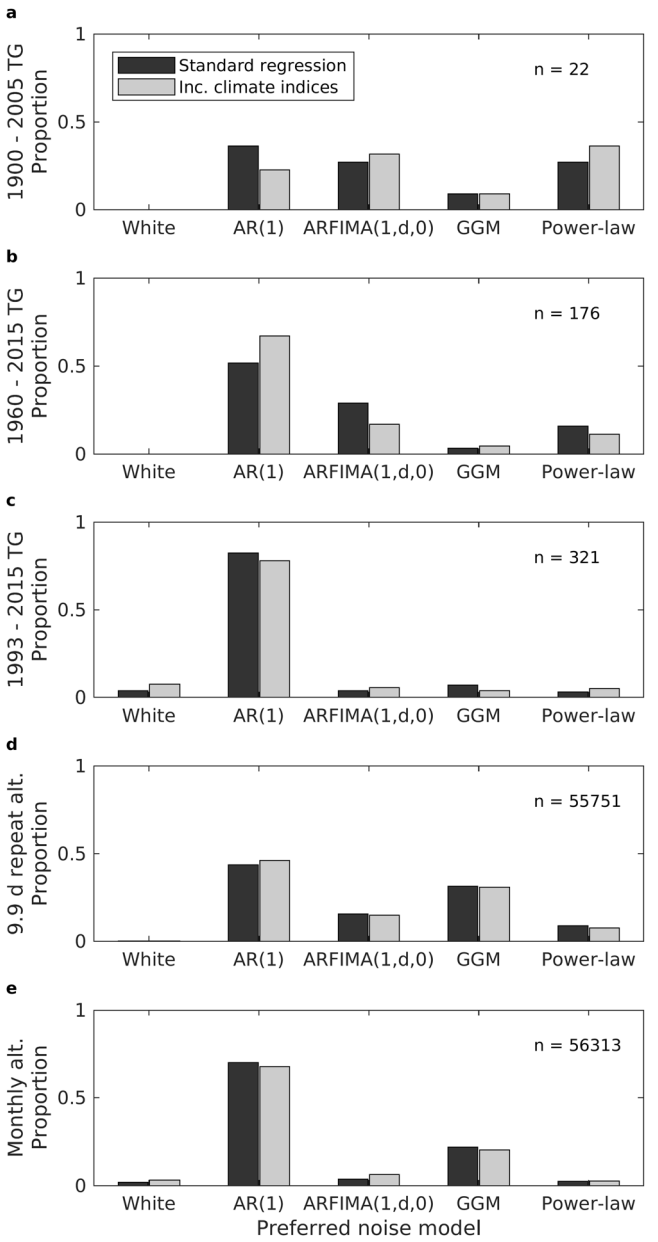

Figure 2. Histograms of the most appropriate noise model type from tide gauge data for the epochs (a) 1993–2015, (b) 1960–2015 and (c) 1900–2005, and from satellite altimetry at (d) 9.9 day repeat and (e) monthly mean, for the standard regression (dark grey) and including climate indices (light grey).

repeat pass frequency are more appropriately described by colored noise models other than AR(1) in 54% (56%) of time series including (excluding) climate indices in the regression.

Therefore, this analysis shows that including climate indices in the multivariate regression significantly affects the trend (refer to ZC12, Figure 4e) but does not substantially affect the most appropriate choice of noise model (Figures 2 and 3), indicating that these climate variables may not represent the dominant noise process.

Figures 3b and 3c show a clear distinction of the most appropriate noise model between equatorial, tropical and mid-latitude regions. In the monthly mean satellite altimetry data, the most appropriate noise model in the equatorial and tropical ($\pm 20^{\circ}$ latitude) regions is best described by AR(1) type models, whereas the noise in the mid tropics to mid-latitudes in the open ocean is often best described by a GGM type model. In the 9.9 day altimetry data, the AR(1) noise model is dominant at the equator, but within the tropics a mixture of AR(1), ARFIMA $(1, d, 0)$, GGM and power-law noise models are most appropriate.

Given sea level observations are an aggregation of numerous geophysical signals, it is not surprising that the noise may be best described by a power-law or integrated noise model, but it is clear that data sets with a smaller number of points can be adequately described by an AR(1) noise model.

We reanalyze the 22 longest duration tide gauge records over the satellite altimetry era (1993–2015). The residual noise from both regression analyses (without and including climate indices) for the shorter sample length is best described by an AR(1) noise in all cases (not shown). Yet considering longer sample lengths of data the most appropriate noise model varies by location.

The sensitivity of the most appropriate noise model selected to the time series duration and sampling frequency may be due to a number of reasons. Since sea level time series exhibit long term memory (a Hurst exponent $H > 0.5$; Dangendorf et al., 2014), it might be expected that a noise model with integrated white noise (such as ARFIMA $(1, d, 0)$ or GGM), for which the auto-covariance sequence decays hyperbolically, should better fit the noise than an AR(1) process, for which the auto-covariance sequence decays exponentially (Hosking, 1981). The preference for the AR(1) model for shorter duration or lower sample frequency data implies a systematic influence of the method applied here. It may be that the smaller number of data points in the time series represent a limit on noise model accuracy and the AIC/BIC scores are dominated by the parsimony principle, choosing the simplest model (AR(1) or power-law) over more complex models (ARFIMA $(1, d, 0)$ or GGM). Additionally, the data set for the altimetry epoch 1993–2015 is shorter than the longest periodicity in the signal and therefore some of the noise could be attributed to a linear trend in the shorter duration data. At high frequencies there is considerable variance in the noise and none of the noise models fit particularly well to the high frequency part of the noise spectra.

Figure 4 presents power spectral density plots for the noise from 4 long duration tide gauges. The effect of the different sample period and climate indices in the regression differs across the sites. At Sydney, San Francisco and Seattle, the noise when including climate indices has reduced power at decadal periods, compared with the noise from the standard regression. There is a consistent reduced power in the noise from the 1993–2015 data set, than the 1900–2005 data set, for Sydney and San Francisco (and to a lesser extent

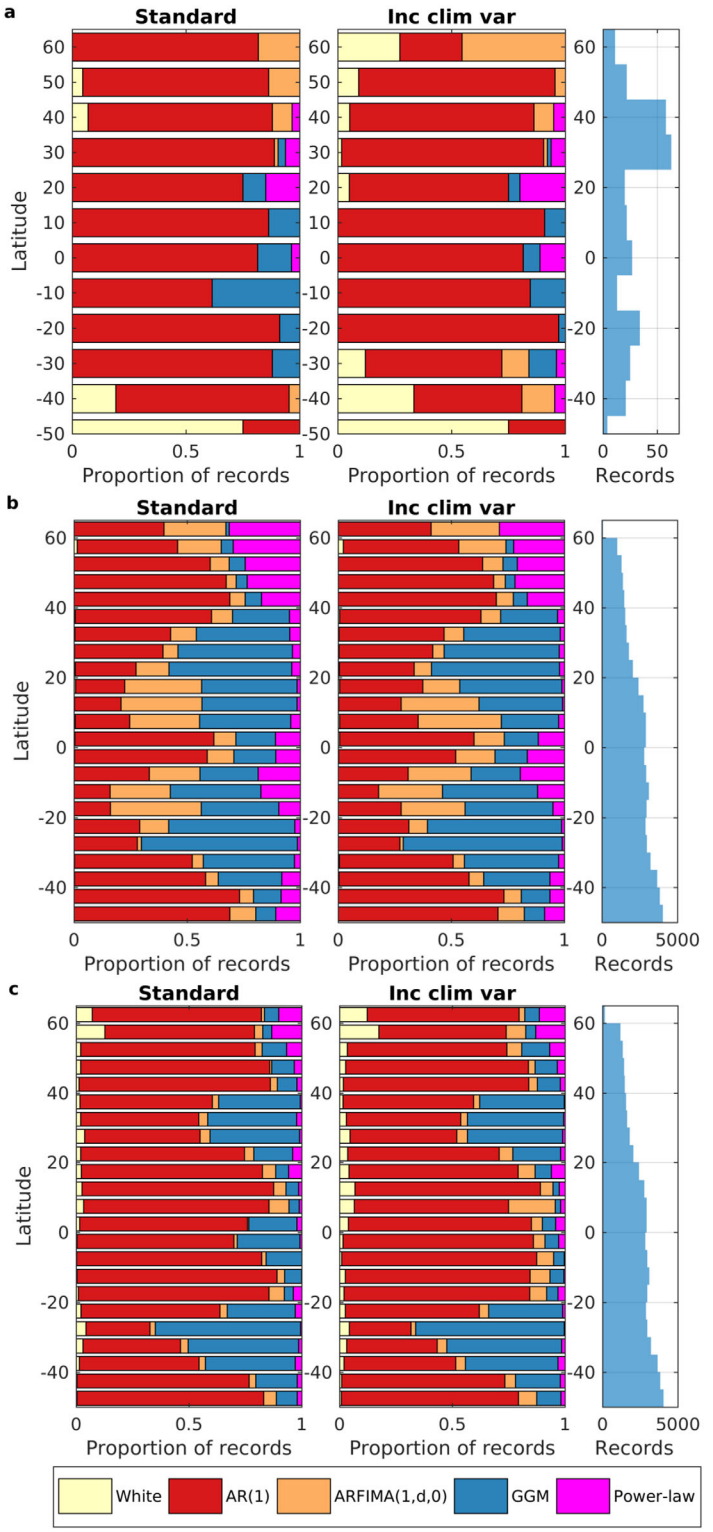

Figure 3. Histograms by latitude of the most appropriate noise model type comparing (left) the standard regression and (middle) including climate indices models. The total count of records is given for information (right): (a) tide gauge data for the epoch 1993–2015, (b) 9.9 day repeat satellite altimetry data, and (c) monthly mean satellite altimetry data.

at Seattle), but it is unclear from the trend coefficient estimates if this power is being erroneously assigned to trend rather than noise. At San Francisco and Seattle, there is a clear reduction in power at the inter-annual frequencies associated with the ICI (the inter-annual periodicity of ENSO). At San Francisco, the preferred noise model is unchanged by including climate indices in the regression (AR(1) for 1993–2015 data and ARFIMA $(1, d, 0)$ for 1900–2005), but the difference in the spectral shape leads to a large variation in the subsequent formal trend error estimates (refer to supporting information Table S3 for full details for the 1900–2005 data set). At Seattle, the reduction in power at inter-annual periods by including climate indices changes the preferred noise model from ARFIMA $(1, d, 0)$ to power-law, substantially increasing the formal trend error estimate. At Honolulu, including climate indices in the 1993–2015 data set has a significant impact on the power in the noise at both inter-annual and decadal periods, which is not apparent in the longer 1900–2005 data set (where the preferred noise model is GGM for both regressions). This is indicative of the issue raised by Frankcombe et al. (2015) whereby the relationship between PDO and ENSO climate indices and sea level is not stationary in time, and may be more pronounced in the more recent past than over the full tide gauge record. Additionally, note the large difference in the trend identified over the 1993–2015 data between the standard regression and that including climate indices, which implies the time series is too short to adequately separate the trend, climate indices and noise components.

The preference for colored but non-AR(1) noise models in the 9.9 day frequency satellite altimetry data, over the monthly data, matches the findings of Bos et al. (2014) where it was found that annual average tide gauge records appear better fit by an AR(1) model. Averaging effectively reduces the high frequency content in the time series, resulting in a smaller bandwidth. This makes it easier for the AR(1) to fit the power spectrum of the residuals, affecting the AIC and BIC scores.

The robustness of the noise model and therefore spectral shape of the noise suggests that the ratio of short-period to long-period spectral energy is only partially affected by the natural climatic variability applied in this study (noting the DCI and ICI here describe variability in the Pacific) and is additionally related to other signals in the sea-level data.

The primary drivers of sea-level change over the instrument record, thermal expansion and mass exchange with the cryosphere and hydrosphere (including terrestrial water storage), exhibit temporal and spatial nonlinearities (Chen et al., 2017; Marzeion et al., 2014; Xue et al., 2012). Furthermore, many geophysical signals will also contribute nonlinearities to the sea-level signal, such as oceanographic physics as described for high frequency by Hughes and Williams (2010). For each time series, the regression applied here accounts for the annual and semi-annual signal in the (local) steric sea level and for a linear relationship with the DCI and ICI indices, which derive from climatic variability in the Pacific. Natural climatic variability not described by a linear relationship with the PDO and ENSO will contribute to the noise term (Palanisamy et al., 2015a). Over the satellite altimetry epoch from 1993 to 2015, the DCI shows a

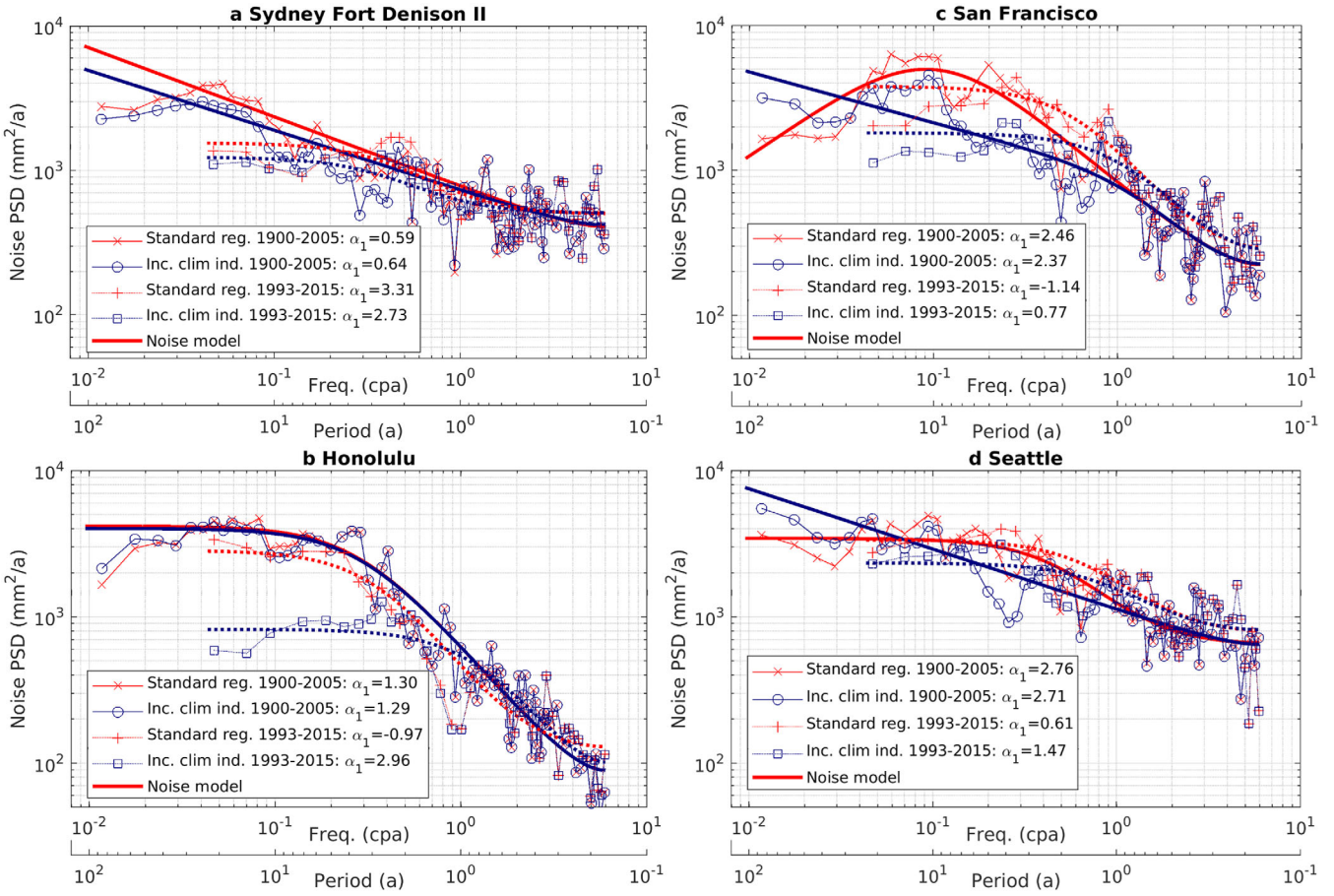

Figure 4. Power spectral density plots of noise for 4 long-duration tide gauge time series, with (blue) and without (red) climate indices included in the regression: (a) Sydney Fort Denison II, (b) Honolulu, (c) San Francisco and (d) Seattle. α_1 is the trend coefficient estimate given in equations (1) and (2).

general decline not wholly independent of a linear trend in time. There may have been a shift in the response of sea level to Pacific variability between the satellite altimetry epoch and earlier epochs (Frankcombe et al., 2015), such that the relationship between sea level and the ICI and DCI is not expected to be constant in time between the epochs investigated here. Considering other climate variates may help more fully represent the drivers of the intrinsic long-period variability in sea-level time series, such as integrated equatorial and longshore wind stress or wind stress curl components (Calafat & Chambers, 2013; Newman et al., 2016; Thompson et al., 2014), but this approach is not feasible for an assessment with basin-scale coverage. Also, natural and human-induced causes of vertical land motion at tide gauges are local and nonlinear in time and will be present in the noise.

4.2. Formal Error Estimates

Allowing for non-AR(1) noise models in a sea-level linear trend regression can significantly effect the formal error estimates for the trend (Bos et al., 2014), and this remains true for our multivariate regression including climate indices. Figure 5 presents histograms of the ratio of the standard error in the trend estimate from the most appropriate noise model, over that from an AR(1) model fit. Ratios greater than 1 represent time series where the trend error is under-estimated if the noise is represented by an AR(1) model, and vice versa. We only present the non-AR(1) ratios for brevity with the number of time series best fit by a non-AR(1) model indicated in each panel. The proportion of time series with standard errors greater or less than those from an AR(1) model varies as a function of the duration and sampling frequency of the data, with variation in the preferred noise model.

For the longest duration tide gauges, 68% of sites have larger standard errors after allowing for non-AR(1) noise models, including climate indices in the regression (45% for standard regression; Table 1). For the

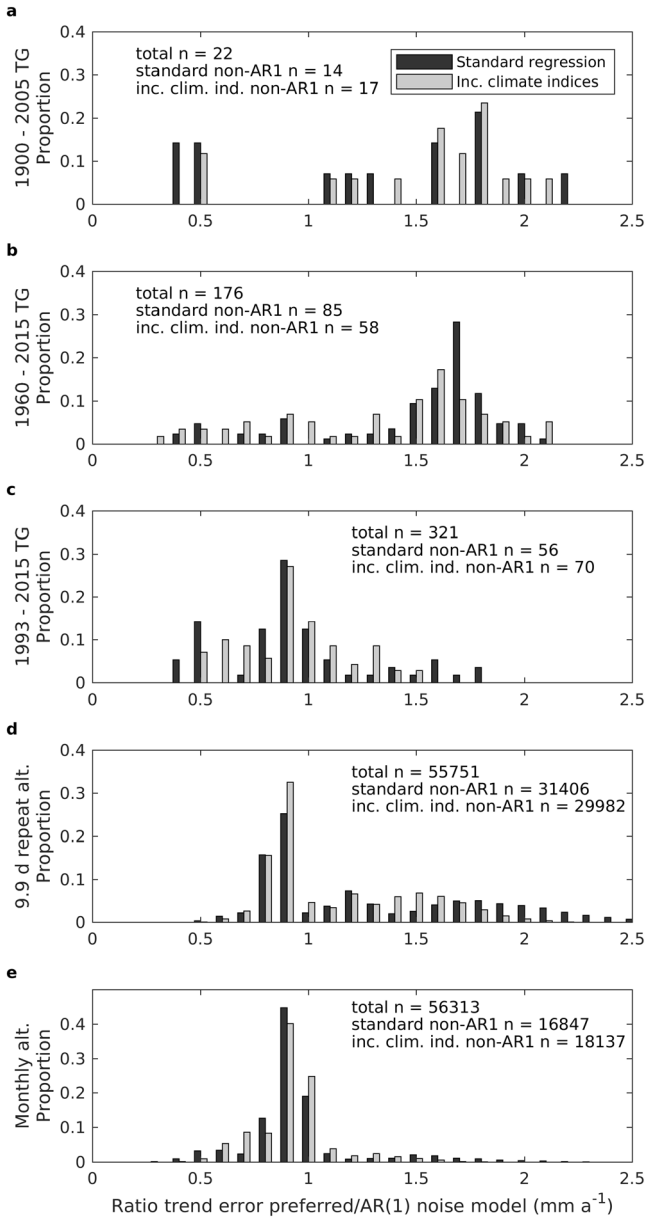

Figure 5. Histograms of the ratio between the standard error from the most appropriate noise model over that from an AR(1) noise model; from tide gauge data for the epochs (a) 1993–2015, (b) 1960–2015 and (c) 1900–2005, and from satellite altimetry at (d) 9.9 day repeat and (e) monthly mean, for the standard regression (dark grey) and including climate indices (light grey).

longest duration tide gauges, including climate indices changes the appropriate noise model for some sites from AR(1) to ARFIMA $(1, d, 0)$ and power-law (Figure 2a). As a result, the median standard error increases to 1.58 times that produced assuming an AR(1) noise model. In all other cases of duration and frequency, the median standard error is equal to that from an AR(1) noise model, but a notable proportion of the records have higher error estimates. For the 9.9 day repeat frequency satellite altimetry data, only 46% of time series are best described with an AR(1) noise model, when including climate indices in the regression (44% for standard regression). In most cases the noise model is colored but not AR(1) and the standard error estimates are greater than those from an AR(1) model in 24% of cases, including climate indices in the regression (30% for standard regression).

The standard error is greatest in regions of high energy, such as the western boundary currents, but also in the equatorial Pacific, the south Tropical Indian Ocean and south-west Tropical Pacific Ocean around the Fiji Basin (Figures 6a and 6e). These later regions exhibit strongly auto-regressive noise (supporting information Figures S4 and S5), which leads to the high error estimates in the MLE approach.

Variations in the most appropriate noise model lead to over- and under-estimates of the trend error. The spatial coherency with latitude in the most appropriate noise model (Figure 3) feeds in to spatial coherency in the ratio of the standard error in the trend compared with assuming an AR(1) noise model, as shown in Figures 6b and 6f. Under-estimates of the trend error correspond to regions where the noise is best described by an ARFIMA $(1, d, 0)$ or power-law noise model, in the satellite altimetry data. Overestimates generally correspond with regions where a GGM noise model is most appropriate. High ratios are also apparent along eastern coastal boundaries (the Americas and Australian west coast), around New Zealand and into the Aleutian Sea. In the monthly mean satellite altimetry data (Figure 6f), the noise in the tropics is generally best described by an AR(1) model. There remain patches of higher standard error around New Zealand and the Aleutian Sea. In both frequency data sets, there is a strong band of lower standard error at 5–10° N in the Pacific Ocean (where the most appropriate noise model is GGM).

The inclusion of climate indices in the regression reduces the standard error in the tropics in line with flattening the noise spectra at low frequencies (Figures 6c and 6g), but leads to an overall increase in the standard error due to the additional degrees of freedom in the model. Large magnitude coefficients are calculated for the DCI and ICI variates in the equatorial and tropical Pacific and Indian Oceans. The DCI variate has large magnitude coefficients into the north Pacific Ocean and on the Australian North West Shelf and along the western coast (supporting information Figure S5). The reduction in standard error by including climate indices is most pronounced where the ICI and DCI indices have largest coefficients in the regression, hence removing the most power from the noise. Aligned with this, the AR(1) coefficient is reduced in these regions, likely due to the reduction in longer period power relative to the 22.7 year duration of the record (supporting information Figure S3). The largest reduction in the standard error corresponds to the equatorial and tropical oceans but also patches of ocean where recent sea-level rise is associated with wind field changes (gyre spin-up and thermocline adjustment) in the south Indian Ocean (Thompson et al., 2016), south-west Pacific Ocean (Roemmich et al., 2016), north-east Pacific Ocean as well as West Australian and Pacific North

Table 1
Proportion of Time Series With Standard Error Estimates Less Than, Equal to, or Greater Than Those Assuming an AR(1) Noise Model

			Proportion		
Data set	Epoch	Regression	Less than	Equal to	Greater than
Tide gauge	1900–2005	Standard	0.18	0.37	0.45
Tide gauge	1900–2005	Inc. climate ind.	0.09	0.23	0.68
Tide gauge	1960–2005	Standard	0.08	0.52	0.40
Tide gauge	1960–2005	Inc. climate ind.	0.10	0.67	0.23
Tide gauge	1993–2015	Standard	0.12	0.83	0.05
Tide gauge	1993–2015	Inc. climate ind.	0.15	0.78	0.07
9.9 day altimetry	1993–2015	Standard	0.26	0.44	0.30
9.9 day altimetry	1993–2015	Inc. climate ind.	0.30	0.46	0.24
Monthly altimetry	1993–2015	Standard	0.24	0.70	0.06
Monthly altimetry	1993–2015	Inc. climate ind.	0.26	0.68	0.06

American coastal sites where coastally-trapped boundary waves propogate equatorial sea-level disturbances (Thompson et al., 2014; White et al., 2014).

The observed trend estimates for the satellite altimetry era 1993–2015 including the DCI and ICI climate indices in the regression are given in Figures 6d and 6h. Stippling indicates regions where the trend is significantly different than zero (to 2 standard errors) using our revised error estimates based on the most appropriate noise model determined by MLE. The standard error estimates in the 9.9 day sample frequency satellite altimetry data are significantly affected by the presence of colored but non-AR(1) noise, whereas the monthly mean data are dominated by AR(1) type noise. But it can be seen that the spatial patterns of regions displaying observed trends significantly different from zero are consistent between these two differently sampled data sets, which are dominated by large observed trend or very quiescent oceans (such as the south-eastern tropical Pacific). The mean trend over the study area for this period is 3.08 mm a^{-1} in both data sets.

4.3. When Does a Trend Emerge From the Intrinsic Noise?

In addition to determining the formal error on a trend estimate, to determine when the trend is different from zero at a given level of statistical significance, it is also interesting to look at the problem of detecting a forced signal within an intrinsically noisy system.

By removing climatic variability associated with the major modes in the Pacific (relating to the PDO and ENSO) and allowing for a range of colored noise models, we improve on estimates of when a given sea-level trend emerges from the noise of the system.

The ToE for the observed trend to emerge from 95% of surrogate stochastic noise time series are presented in Figure 7, parameterized from the multivariate regression including climate indices over the satellite altimetry era (1993–2015). The mean of the observed trend from the satellite altimetry in this period and this region is 3.08 mm a^{-1}. The ToE varies from less than 20 to 100 years, associated with regions of lower to higher variability and hence standard error (Figures 6b, 6f, 7b, and 7f), with a mean ToE over this region of 66 (76) years for the monthly mean (9.9 day repeat) satellite altimetry data. The ToE for the observed trend is greater than 50 years for 64% (78%) of the Pacific and Indian Ocean covered in this analysis from the monthly mean (9.9 day repeat) satellite altimetry data. These time scales are much higher than equivalent model studies because the observations have much greater high frequency variation than climate models.

The ToE determined from the most appropriate noise model varies by up to 6 years compared with an AR(1) model, in satellite altimetry data, with an incoherent spatial distribution (Figures 7c and 7g). This difference is dictated by the spread in the distribution of ToE values obtained over the 1,000 surrogate noise time series for different noise models (supporting information Figure S2). Taking the mean observed trend of 3.08 mm a^{-1} (including climate indices in the regression), the lower magnitude of residual noise reduces the ToE by up to 2 decades (compare Figures 7d and 7h with Figures 6d and 6h).

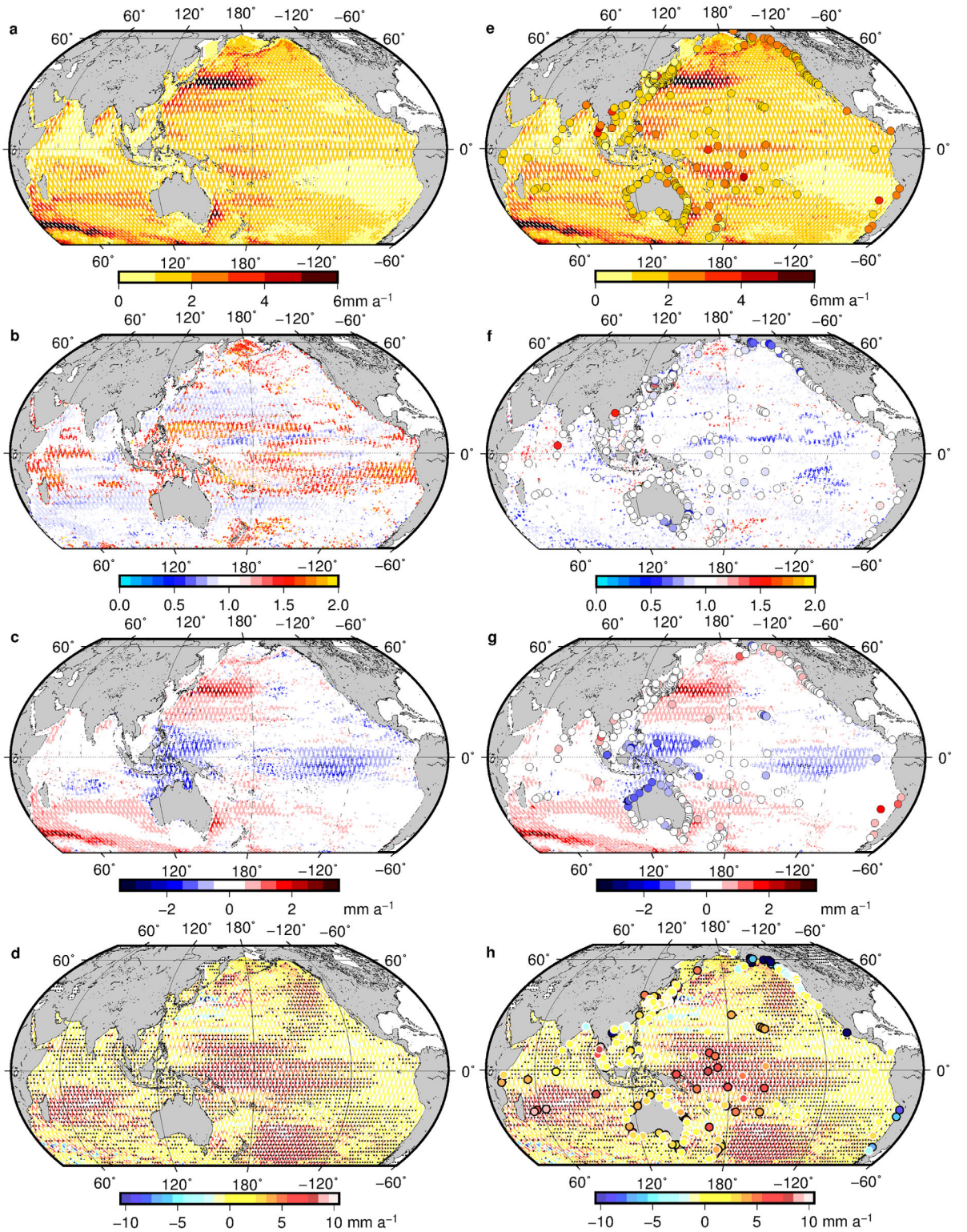

Figure 6. Standard errors and the observed trend estimates for regression including (left) climate indices on 9.9 day repeat satellite altimetry and (right) monthly mean satellite altimetry and 1993–2015 tide gauge data: (a, e) one standard error (mm a^{-1}) from the MLE assessment assuming an AR(1) noise model; (b, f) the ratio of the standard error from the most appropriate noise model to that from an AR(1) noise model; (c, g) the difference in the standard error (mm a^{-1}) from MLE assessment with the most appropriate noise model due to the inclusion of climate indices in the regression; and (d, h) observed trend (mm a^{-1}). Tide gauge data are shown as filled circles. In Figures 6d and 6h stippling over the altimetry data and tide gauge symbols with a black border indicate the observed trend is significantly different from zero (2 s.e.).

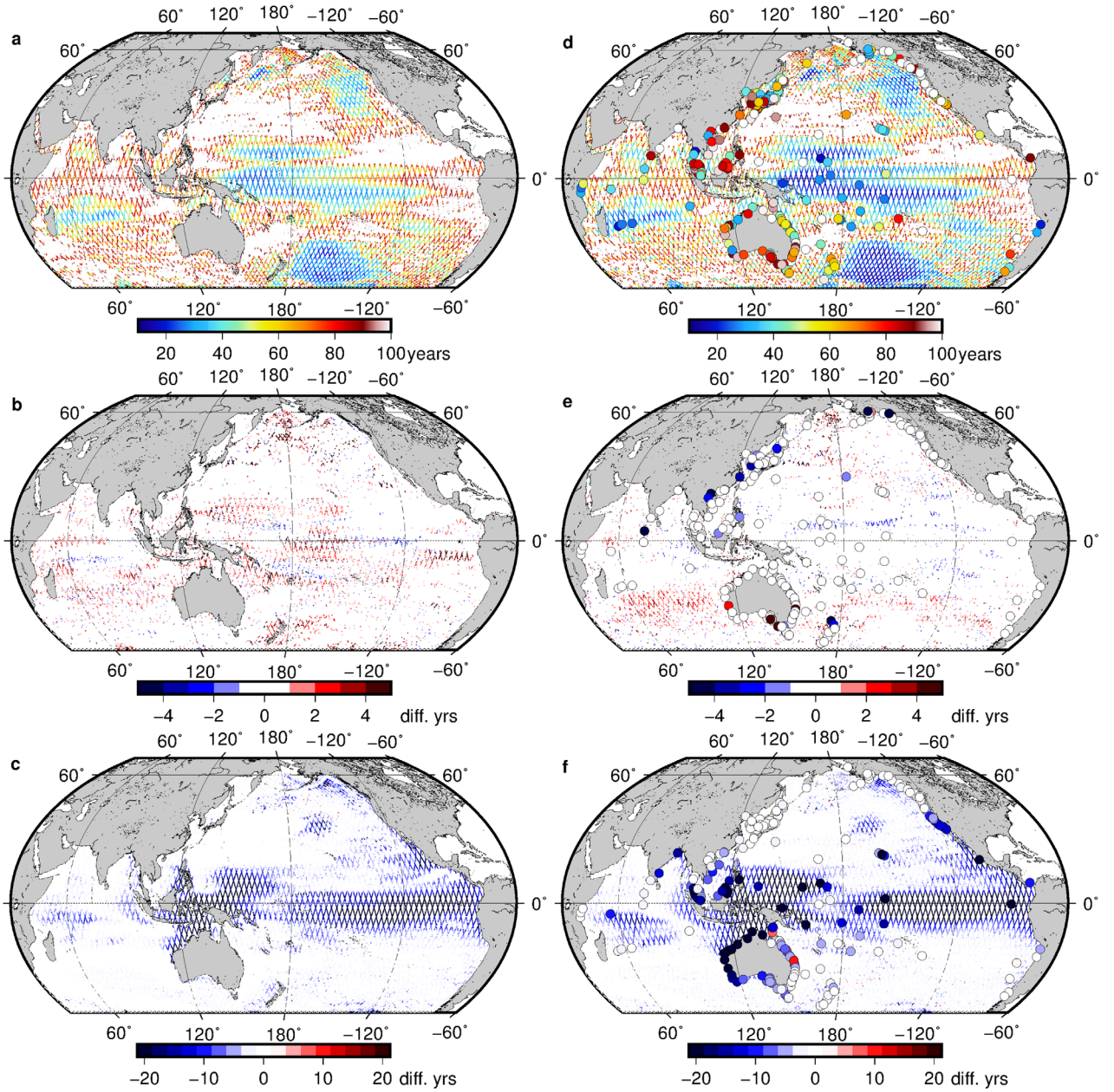

Figure 7. Time of emergence, ToE, (a) for a given magnitude trend to emerge from 95% of surrogate stochastic noise time series. (left) 9.9 day repeat satellite altimetry and (right) monthly mean satellite altimetry and 1993–2015 tide gauge data: (a, d) ToE for the observed trend from 1993–2015, (b, e) the difference in the ToE from the most appropriate noise model against an AR(1) noise model for the observed trend, and (c, f) the difference in the ToE due to including climate variables in the regression for the observed trend. Tide gauge data are shown as filled circles.

In Figure 8, the observed trend from the regression model including climate indices is presented, together with regions where the trend emerges from 50%, 75% and 95% of surrogate stochastic noise time series over the same period as the observations (22.7 years).

By including DCI and ICI climate indices as variates in the regressions for data in the altimetry era the east-west see-saw of sea-level trends is somewhat leveled, particularly in the equatorial zone, as discussed by ZC12 (Figure 8). With 22.7 years of altimetry data, we now find that the very large positive trend immediately to the east of the Philippines (between longitudes 120° E and 140° E) is reduced to be insignificant from zero by including climate indices in the regression.

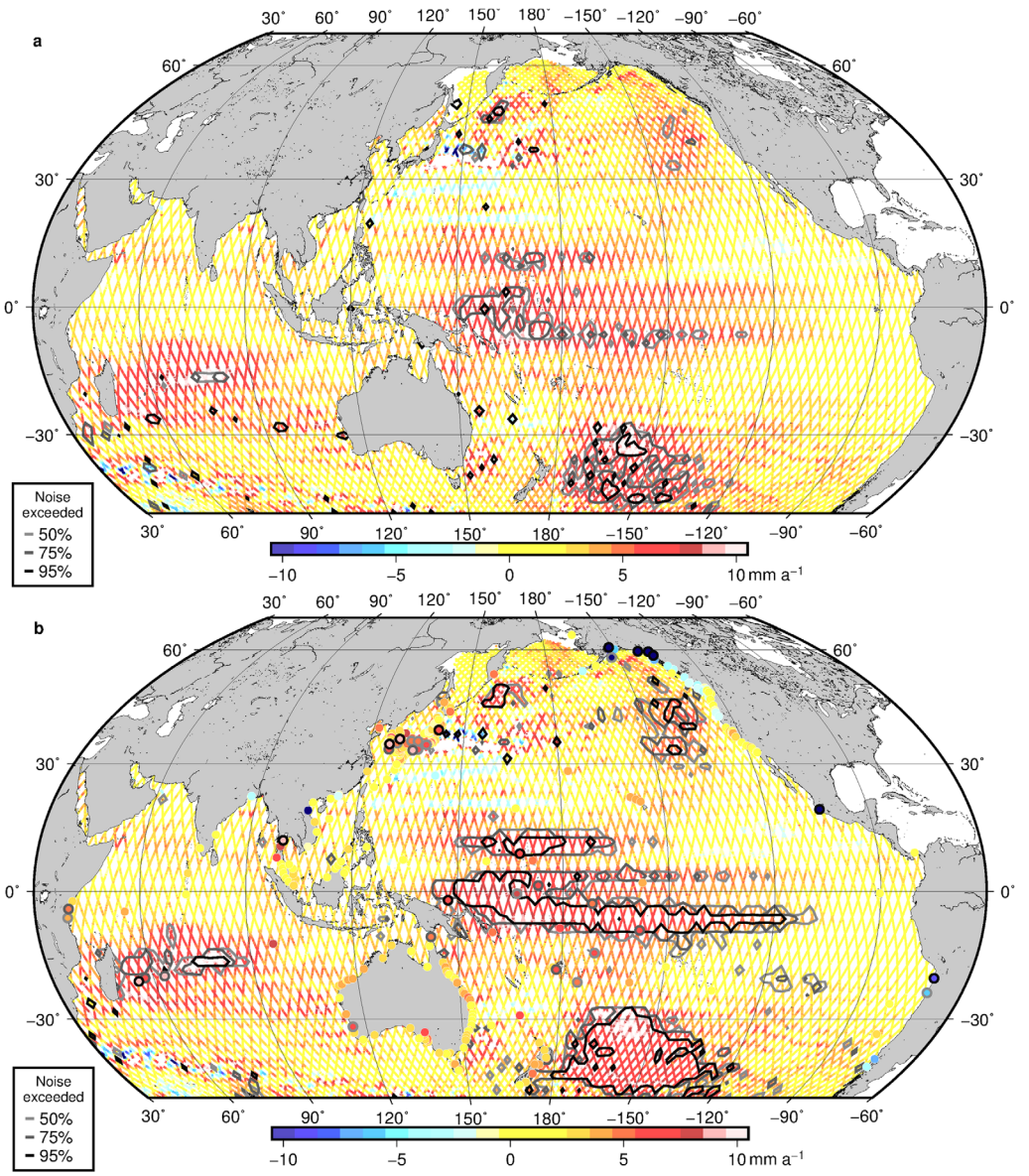

Figure 8. Observed sea-level trend (mm a^{-1}) for (a) 9.9 day repeat satellite altimetry, and (b) monthly mean satellite altimetry and 1993–2015 tide gauge data. Observed trend over the satellite altimetry era 1993–2015, including climate indices in the regression. Light to dark grey contours highlight regions where the observed trend exceeds 50%, 75% and 95% respectively of surrogate noise time series within 22.7 years.

There is a clear decrease in the extent where the observed trend exceeds the noise with an increasing percentage of surrogates exceeded. There is an even chance (50% of surrogates exceeded; Figure 8) that the observed trends across large areas of the equatorial and tropical Pacific Ocean, the south-west Pacific gyre off New Zealand, the north-east Pacific gyre, and, the tropical south-west Indian Ocean off Madagascar, exceed the noise within the available data duration. The gyre regions have been noted as regions of recent increased sea-level rise, spun-up by changes in wind stress (Roemmich et al., 2016; Thompson et al., 2016). Similarly, changes to the wind stress regime have been linked to thermohaline adjustment leading to increased sea-level rise in the tropical Pacific Ocean (Palanisamy et al., 2015b; Peyser et al., 2016). It is noted in this analysis, the trend and noise in the majority of these regions are modified by the inclusion of climate indices in the regression, aiding the signal-to-noise ratio. An exception is the south-west Pacific gyre located to the east of New Zealand, which shows a large magnitude positive trend and colored, but non-AR(1),

noise that is not affected by the DCI and ICI in this analysis. Here applying different co-variates in the regression could improve the signal-to-noise ratio further.

However, the distribution of ToE for a given location from the 1,000 sample surrogates can be significantly spread, particularly when the most appropriate noise model is ARFIMA$(1, d, 0)$ or power-law (supporting information Figure S2). As a result, a more conservative threshold of 95% of surrogate noise time series exceeded leads to considerably smaller regions with an observed trend from the satellite altimetry era exceeding the noise (Figure 8). For the monthly mean satellite altimetry data, 14.6% of the Pacific and Indian Oceans' time series covered in this analysis exhibit an observed trend that is greater than 50% of the surrogate noise time series, decreasing to 11.1% and 6.4% exceeding 75% and 95% of surrogate noise time series. For the 9.9 day repeat satellite altimetry data, only 5.1%, 3.2% and 1.5% of the time series' observed trends exceed 50%, 75% and 95% respectively of the surrogate noise time series.

As discussed in section 4.1, the most appropriate noise model is sensitive to the length of the sea-level time series record. It should be expected that, as the length of satellite altimetry data increases, a colored but non-AR(1) noise model will more often best describe the noise and therefore, the emergence of the trend for the monthly mean satellite altimetry data (Figure 8b) may under-estimate the true intrinsic variability and overestimate the areal extent where a sea-level rise signal exceeds the noise.

With 22.7 years of satellite altimetry data, there are only two regions where the observed trend exceeds 95% of the surrogate noise time series (highlighted by stippling in Figure 8). In both the 9.9 day and monthly mean altimetry data, the south-west Pacific gyre is apparent. In the monthly mean data, there is a band of observed trends significantly exceeding the intrinsic noise in the central Pacific Ocean, around 10° S and across the equator in the western tropical Pacific Ocean. For the long-duration tide gauge time series, the observed trends over the full length of data are generally lower than those from the satellite altimetry era (supporting information Figure S6). Therefore, there are a number of tide gauges for the epoch 1900–2005 where the signal-to-noise ratio is small and the ToE is of the order of 100 years.

5. Conclusions

Large uncertainties in trend estimates are not only limited to regions of high energy and therefore to high variance in the sea-level anomaly time series. Large uncertainties in a linear trend estimate also occur where the residual noise is temporally-correlated and highly nonlinear.

Previous work has demonstrated the colored nature of noise in sea-level time series (Bos et al., 2014; Burgette et al., 2013; Hughes & Williams, 2010). Here we further show that the inclusion of indices representing key modes of Pacific climate variability in a regression analysis: (i) only lessens the auto-regressive noise coefficient in the tropics and along certain coastlines, and (ii) does not significantly affect the most appropriate noise model.

In most regions of the open ocean in the 9.9 day repeat satellite altimetry data and in long tide gauge records, the residual noise is characteristically colored, but non-AR(1). Trend error estimates assuming a noise model that best fits the residual differ from those from AR(1) noise models, with between 30% smaller and 58% larger error estimates depending on the duration and frequency of the observation data set. The error estimates increase by a ratio of up to 1.6 for long-duration tide gauges.

The variability demonstrated here of the most appropriate noise model by the frequency and span of the sea-level data set indicates that the underlying noise process is integrated (and therefore best described by a colored but non-AR(1) noise model), where an AR(1) noise model is an adequate approximation over shorter spans of data. When using the sample resolution satellite altimetry data, long duration tide gauge time series, or, as satellite altimetry data have longer coverage, we should expect the time series to be best described by non-AR(1) noise models, giving different trend error uncertainties.

Using these noise models we simulate when a given trend emerges, and remains outside of, 1,000 sample surrogate noise time series, identifying regions where the observed trend exceeds that which could be produced by the intrinsic noise in the system. There is an even chance that the observed trends exceed the intrinsic noise (exceeds 50% of the surrogate noise time series) for substantial areas of the Pacific and Indian Oceans, that are known to have enhanced recent sea-level rise due to intensification or changes in wind

stress regimes. Given that the most appropriate noise model for longer sea-level time series is colored, but non-AR(1), the extents given by the 9.9 day repeat frequency data are more robust to the noise model type than the monthly mean data.

Including climate indices in a multivariate regression lessens the spectral power of the residual noise at inter-annual and greater periods in the tropics and along waveguides and reduces the time taken for a given trend to emerge from the noise by up to 2 decades. The effect of colored, but non-AR(1), noise generally changes the ToE by a few years.

Even when allowing for PDO and ENSO related Pacific climatic variability in the regression to improve the signal-to-noise ratio, only the central tropical Pacific Ocean, extending eastward to the south of the equator and the south-west Pacific gyre off New Zealand, presently exhibit estimated trends that exceed 95% of the surrogate noise time series over the satellite altimetry period (1993–2015). Extending this analysis for other modes of natural variability could reduce the signal-to-noise ratio and provide improved ToE estimates for sea-level trends in additional regions. The small extent of these regions is due to the increased spread in the ToE distribution across the 1,000 sample surrogate noise time series, that is greater for colored, but non-AR(1), noise models. Thus, the methodology gives high confidence that the satellite altimetry data in these regions contain a sea-level rise signal additional to PDO and ENSO variability and the inherent noise.

Acknowledgments

Appreciation is given to Nate Mantua and the University of Washington for hosting the Pacific Decadal Oscillation (PDO) time series; to Klaus Wolter and NOAA ESRL for hosting the Multivariate ENSO Index (MEI) time series; to AVISO and the CMEMS for providing DUACS altimeter data; and, the Permanent Service for Mean Sea Level (PSMSL) for hosting monthly mean tide gauge time series. Hector v1.6 is available to download from Universidade da Beira Interior at http://segal.ubi.pt/hector/. The parameter estimation for the noise models and trend estimation presented in this paper are provided in the supporting information Datasets. Alternative data formats can be requested from the corresponding author. We acknowledge the use of GMT in a number of figures (Wessel et al., 2013). This work was supported by an Australian Research Council Discovery Project (ID DP150100615). MAK was additionally supported by an Australian Research Council Future Fellowship (FT110100207). BL was supported by the NESP Earth System and Climate Change Hub. MB was sponsored by National Portuguese funds through FCT in the scope of the project IDL-FCT-UID/GEO/50019/2013 and grant SFRH/BPD/89923/2012.

References

Akaike, H. (1973). Information theory and an extension of the maximum likelihood principle. In B. N. Petrov and S. Caski (Eds.), *Proceedings of the second international symposium on information theory* (pp. 267–281). Budapest: Akadémiai Kiado.

Bos, M., & Fernandes, R. (2016). *Hector user manual version 1.6* (Tech. Rep.). Covilhã, Portugal: SEGAL Universidade da Beira Interior.

Bos, M. S., Fernandes, R. M. S., Williams, S. D. P., & Bastos, L. (2008). Fast error analysis of continuous GPS observations. *Journal of Geodesy*, *82*(3), 157–166. https://doi.org/10.1007/s00190-007-0165-x

Bos, M. S., Fernandes, R. M. S., Williams, S. D. P., & Bastos, L. (2013). Fast error analysis of continuous GNSS observations with missing data. *Journal of Geodesy*, *87*(4), 351–360. https://doi.org/10. 1007/s00190-012-0605-0

Bos, M. S., Williams, S. D. P., Araújo, I. B., & Bastos, L. (2014). The effect of temporal correlated noise on the sea level rate and acceleration uncertainty. *Geophysical Journal International*, *196*(3), 1423–1430. https://doi.org/10.1093/gji/ggt481

Burgette, R. J., Watson, C. S., Church, J. A., White, N. J., Tregoning, P., & Coleman, R. (2013). Characterizing and minimizing the effects of noise in tide gauge time series: Relative and geocentric sea level rise around Australia. *Geophysical Journal International*, *194*(2), 719–736. https://doi.org/10.1093/gji/ggt131

Calafat, F. M., & Chambers, D. P. (2013). Quantifying recent acceleration in sea level unrelated to internal climate variability. *Geophysical Research Letters*, *40*, 3661–3666. https://doi.org/10.1002/grl. 50731

Chen, X., Zhang, X., Church, J. A., Watson, C. S., King, M. A., Monselesan, D., et al. (2017). The increasing rate of global mean sea-level rise during 1993–2014. *Nature Climate Change*, *7*, 492–495. https://doi.org/10.1038/nclimate3325

Dangendorf, S., Marcos, M., Müller, A., Zorita, E., Riva, R., Berk, K., & Jensen, J. (2015). Detecting anthropogenic footprints in sea level rise. *Nature Communications*, *6*, 7849. https://doi.org/10.1038/ncomms8849

Dangendorf, S., Rybski, D., Mudersbach, C., Müller, A., Kaufmann, E., Zorita, E., & Jensen, J. (2014). Evidence for long-term memory in sea level. *Geophysical Research Letters*, *41*, 5530–5537. https://doi.org/10.1002/2014GL060538

Emery, W. J., & Thomson, R. E. (2001). *Data analysis methods in physical oceanography*. New York, NY: Elsevier Science.

Frankcombe, L. M., McGregor, S., & England, M. H. (2015). Robustness of the modes of Indo-Pacific sea level variability. *Climate Dynamics*, *45*(5), 1281–1298. https://doi.org/10.1007/s00382-014-2377-0

Haigh, I. D., Wahl, T., Rohling, E. J., Price, R. M., Pattiaratchi, C. B., Calafat, F. M., & Dangendorf, S. (2014). Timescales for detecting a significant acceleration in sea level rise. *Nature Communications*, *5*, 3635. https://doi.org/10.1038/ncomms4635

Hamlington, B. D., Leben, R. R., & Kim, K.-Y. (2012). Improving sea level reconstructions using non-sea level measurements. *Journal of Geophysical Research*, *117*, C10025. https://doi.org/10.1029/2012JC008277

Hamlington, B. D., Leben, R. R., Nerem, R. S., Han, W., & Kim, K.-Y. (2011). Reconstructing sea level using cyclostationary empirical orthogonal functions. *Journal of Geophysical Research*, *116*, C12015. https://doi.org/10.1029/2011JC007529

Hamlington, B. D., Strassburg, M. W., Leben, R. R., Han, W., Nerem, R. S., & Kim, K.-Y. (2014). Uncovering the anthropogenic sea-level rise signal in the Pacific Ocean. *Nature Climate Change*, *4*, 782–785. https://doi.org/10.1038/nclimate2307

Harrison, C. G. A. (2002). Power spectrum of sea level change over fifteen decades of frequency. *Geochemistry, Geophysics, Geosystems*, *3*(8), 10047. https://doi.org/10.1029/2002GC000300

Holgate, S. J., Matthews, A., Woodworth, P. L., Rickards, L. J., Tamisiea, M. E., Bradshaw, E., et al. (2013). New data systems and products at the Permanent Service for Mean Sea Level. *Journal of Coastal Research*, *29*(3), 493–504. https://doi.org/10.2112/JCOASTRES-D-12-00175.1

Hosking, J. R. M. (1981). Fractional differencing. *Biometrika*, *68*(1), 165–176.

Hughes, C. W., & Williams, S. D. P. (2010). The color of sea level: Importance of spatial variations in spectral shape for assessing the significance of trends. *Journal of Geophysical Research*, *115*, C10048. https://doi.org/10.1029/2010JC006102

Jordá, G. (2014). Detection time for global and regional sea level trends and accelerations. *Journal of Geophysical Research: Oceans*, *119*, 7164–7174. https://doi.org/10.1002/2014JC010005

Langbein, J. (2004). Noise in two-color electronic distance meter measurements revisited. *Journal of Geophysical Research*, *109*, B04406. https://doi.org/10.1029/2003JB002819

Lyu, K., Zhang, X., Church, J. A., Slangen, A. B. A., & Hu, J. (2014). Time of emergence for regional sea-level change. *Nature Climate Change*, *4*(11), 1006–1010. https://doi.org/10.1038/nclimate2397

Mantua, N. (2016). *PDO index*. Retrieved from research.jisao.washington.edu/pdo/PDO.latest, last accessed May 2016

Marzeion, B., Cogley, J. G., Richter, K., & Parkes, D. (2014). Attribution of global glacier mass loss to anthropogenic and natural causes. *Science*, *345*(6199), 919–921. https://doi.org/10.1126/science.1254702

Mertz, F. M., Pujol, M. I., & Faugere, Y. (2017). *Copernicus Marine Environment Monitoring Service Product User Manual for sea level SLA products* (Tech. Rep no. MYO2-SL-PUM008-001-005). Toulouse, France: CMEMS.

Meyssignac, B., Salas y Melia, D., Becker, M., Llovel, W., & Cazenave, A. (2012). Tropical pacific spatial trend patterns in observed sea level: Internal variability and/or anthropogenic signature? *Climate of the Past*, *8*(2), 787–802. https://doi.org/10.5194/cp-8-787-2012

Newman, M., Alexander, M., Ault, T., Cobb, K., Deser, C., Lorenzo, E. D., et al. (2016). The Pacific Decadal Oscillation, revisited. *Journal of Climate*, *29*(12), 4399–4427. https://doi.org/10.1175/JCLI-D-15-0508.1

NOAA ESRL. (2016a). Multi-variate ENSO index. Retrieved from www.esrl.noaa.gov/psd/enso/mei/table.html (last accessed August 2016).

NOAA ESRL (2016b). Extended multi-variate ENSO index. Retrieved from www.esrl.noaa.gov/psd/enso/mei.ext/table.ext.html (last accessed August 2016).

Palanisamy, H., Cazenave, A., Delcroix, T., & Meyssignac, B. (2015b). Spatial trend patterns in the pacific ocean sea level during the altimetry era: The contribution of thermocline depth change and internal climate variability. *Ocean Dynamics*, *65*(3), 341–356. https://doi.org/10.1007/s10236-014-0805-7

Palanisamy, H., Meyssignac, B., Cazenave, A., & Delcroix, T. (2015a). Is anthropogenic sea level fingerprint already detectable in the Pacific Ocean? *Environmental Research Letters*, *10*(8), 084024.

Peyser, C. E., Yin, J., Landerer, F. W., & Cole, J. E. (2016). Pacific sea level rise patterns and global surface temperature variability. *Geophysical Research Letters*, *43*, 8662–8669. https://doi.org/10.1002/2016GL069401

PSMSL. (2017). RLR monthly tide gauge data. Retrieved from www.psmsl.org/data/obtaining/ (last accessed 27 Feb 2017).

Richter, K., & Marzeion, B. (2014). Earliest local emergence of forced dynamic and steric sea-level trends in climate models. *Environmental Research Letters*, *9*(11), 114009. https://doi.org/10.1088/1748-9326/9/11/114009

Roemmich, D., Gilson, J., Sutton, P., & Zilberman, N. (2016). Multidecadal change of the South Pacific gyre circulation. *Journal of Physical Oceanography*, *46*(6), 1871–1883. https://doi.org/10.1175/JPO-D-15-0237.1

Schwarz, G. (1978). Estimating the dimension of a model. *The Annals of Statistics*, *6*(2), 461–464.

Thompson, P. R., Merrifield, M. A., Wells, J. R., & Chang, C. M. (2014). Wind-driven coastal sea level variability in the northeast Pacific. *Journal of Climate*, *27*(12), 4733–4751. https://doi.org/10.1175/JCLI-D-13-00225.1

Thompson, P. R., Piecuch, C. G., Merrifield, M. A., McCreary, J. P., & Firing, E. (2016). Forcing of recent decadal variability in the Equatorial and North Indian Ocean. *Journal of Geophysical Research: Oceans*, 121, 6762–6778. https://doi.org/10.1002/2016JC012132

von Storch, H., & Zwiers, F. (1999). *Statistical analysis in climate research*. Cambridge, UK: Cambridge University Press.

Wessel, P., Smith, W. H. F., Scharroo, R., Luis, J. F., & Wobbe, F. (2013). Generic mapping tools: Improved version released. *Eos, Transactions of American Geophysical Union*, *94*, 409–410.

White, N. J., Haigh, I. D., Church, J. A., Koen, T., Watson, C. S., Pritchard, T. R., et al. (2014). Australian sea levels–Trends, regional variability and influencing factors. *Earth-Science Reviews*, *136*, 155–174. http://doi.org/10.1016/j.earscirev.2014.05.011

Wolter, K., & Timlin, M. S. (1993). Monitoring ENSO in COADS with a seasonally adjusted principal component index. In *Proceedings of the 17th climate diagnostics workshop* (pp. 52–57). Norman, OK: NOAA/NMC/CAC.

Wolter, K., & Timlin, M. S. (2011). El Niño/Southern Oscillation behaviour since 1871 as diagnosed in an extended multivariate ENSO index (mei.ext). *International Journal of Climatology*, *31*(7), 1074–1087. https://doi.org/10.1002/joc.2336

Xue, Y., Balmaseda, M. A., Boyer, T., Ferry, N., Good, S., Ishikawa, I., et al. (2012). A comparative analysis of upper-ocean heat content variability from an ensemble of operational ocean reanalyses. *Journal of Climate*, *25*(20), 6905–6929. https://doi.org/10.1175/JCLI-D-11-00542.1

Zhang, X., & Church, J. A. (2012). Sea level trends, interannual and decadal variability in the Pacific Ocean. *Geophysical Research Letters*, *39*, L21701. https://doi.org/10.1029/2012GL053240

Zhang, Y., Wallace, J. M., & Battisti, D. S. (1997). ENSO-like interdecadal variability: 1900-93. *Journal of Climate*, *10*, 1004–1020.